Adjoint-based sensitivity analysis and assimilation of multi-source data for the inference of spatio-temporal parameters in a 2D urban flood hydraulic model

Léo Pujol, Pierre-André Garambois, Carole Delenne, Jean-Louis Perrin

▶ **To cite this version:**

Léo Pujol, Pierre-André Garambois, Carole Delenne, Jean-Louis Perrin. Adjoint-based sensitivity analysis and assimilation of multi-source data for the inference of spatio-temporal parameters in a 2D urban flood hydraulic model. 2024. hal-04643149

HAL Id: hal-04643149
https://hal.science/hal-04643149

Preprint submitted on 10 Jul 2024

HAL is a multi-disciplinary open access archive for the deposit and dissemination of scientific research documents, whether they are published or not. The documents may come from teaching and research institutions in France or abroad, or from public or private research centers.

L'archive ouverte pluridisciplinaire **HAL**, est destinée au dépôt et à la diffusion de documents scientifiques de niveau recherche, publiés ou non, émanant des établissements d'enseignement et de recherche français ou étrangers, des laboratoires publics ou privés.

Distributed under a Creative Commons Attribution - ShareAlike 4.0 International License

Adjoint-based sensitivity analysis and assimilation of multi-source data for the inference of spatio-temporal parameters in a 2D urban flood hydraulic model

Léo Pujol[a,*], Pierre-André Garambois[b], Carole Delenne[a,c] and Jean-Louis Perrin[a]

[a]HydroSciences Montpellier, Univ. Montpellier, CNRS, IRD, Montpellier, 34000, France
[b]INRAE, RECOVER, Aix-Marseille Université, Aix-en-Provence, 13100, France
[c]Inria, team Lemon, Montpellier, 34000, France

ARTICLE INFO

Keywords:
2D Shallow Water model
Urban Flash Flood
Variational Data Assimilation
High-Water Marks
Sensitivity Maps
Derivative-Based Global Sensitivity Measures (DGSM)

ABSTRACT

This contribution presents a novel approach for the calibration of distributed parameters in a 2D urban flood hydraulic model. It focuses on the challenging issue of inferring distributed friction parameters from multi-source heterogeneous spatio-temporal observations of their hydraulic signatures in the context of an urban flash flood in a complex street network. A variational data assimilation algorithm is used to infer high-dimensional multi-variate parameters (spatialized friction and inflow discharge time series) using multi-source observations. This method relies on a differentiable 2D shallow water hydraulic model which enables to generate high-resolution sensitivity maps of local gradients and Derivative-based Global Sensitivity Measures (DGSM), enabling to guide adequate definition of parameter spatialization for the data assimilation process. Assimilated data include real local limnigraphic measurements and high-water marks collected after a major flood event, as well as modeled flow velocity used in twin experiments setups. This study is the first to leverage high-water marks with a variational method for the calibration of distributed parameters in an urban flood model. The multi-source data is used to infer inflow hydrographs and distributed friction parameters in setups of varying complexity. In the main setup, the complex structure of the street network, along with the sensitivity maps and hydraulics expertise led to define a model configuration with 45 friction patches. A high-dimensional parameter vector composed of these friction values and an upstream inflow is inferred simultaneously by assimilating real limnigraphic data and high-water marks. This leads to an increase in model fit to observations and satisfying parameter estimates.

1. Introduction

In the context of global change, the potential increase in frequency and intensity (Masson-Delmotte et al. (2022)) of extreme rainfall events may lead to an increase in flood occurrences. Urbanization is linked to the sealing of natural soils, which may lead to increased flood impacts in densely populated areas (Ogden et al., 2011). Furthermore, the multiplicity of flow paths with complex geometries in urban areas makes the study of urban floods at High Resolution (HR) a challenge and a necessity Bulti and Abebe (2020). Understanding urban flows and improving our capability to predict urban floods is a key issue for the protection of populations, and prediction tools should rely on HR hydraulic models able to accurately model complex flows and to leverage heterogeneous data sources (Mignot and Dewals (2022)).

The hydrodynamic phenomena at play in urban floods are potentially rapidly varied in space and time. The interaction of relatively energetic flows with street networks and local geometries can trigger complex flood flows,

leo.pujol@ird.fr (L. Pujol)
ORCID(s): 0000-0002-8903-1270 (L. Pujol)

which makes the modeling of urban floods particularly challenging. Local geometries can refer to culverts, street intersections, obstacles such as cars or urban furniture which can all generate losses of mechanical flow energy. Urban flood flows can be highly non-linear and model response can be sensitive to local controls, as studied through friction sensitivity analysis in urban hydraulic models of urban floods in Chen et al. (2018) and through detailed hydraulic signatures analysis of an experimental street network dataset in (Finaud-Guyot et al., 2018, 2019). This sensitivity is not easily measurable or localizable on real cases (Mignot and Dewals, 2022). Modeling the influence of fine-scale topography and complex geometries on flood flows can be performed with a 2D hydraulic modeling approach (see e.g. model validations in (Arrault et al., 2016; Chen et al., 2018; Dellinger et al., in prep.) using experimental data from (Finaud-Guyot et al., 2018, 2019), see also references in review of Mignot and Dewals (2022)). Still, building and better constraining such models from heterogeneous data remains a challenge.

Indeed, building HR urban flood models requires HR data to describe fine spatial variations of topography and hydraulic structures, as well as estimations of hydrological inflows and real flow data to estimate the unobservable hydraulic friction which models flow momentum dissipation and is also often used to compensate modeling errors. A key challenge that pertains to flow observation availability stems from the multi-scale aspect of flow variability and the difficulty of adequately observing it, in part because of the localized, sudden and violent nature of most floods. Indeed, observations of the local impacts of complex geometries on flow is difficult to acquire, while observations of the larger scale impacts of friction effects may be more readily available. Therefore, it becomes necessary to adopt modeling approaches of appropriate complexity that are capable of leveraging any available data, which requires methods for the assimilation of heterogeneous, uncertain distributed observations of flow signals.

A growing wealth of information provided by multi-sensors measurements is exploitable to build and to better constrain HR hydraulic models, as explored in recent works. To build a model, accurate topography – vital to HR modeling – can be derived from remote-sensed data like HR LiDAR for urban models, see e.g. Haile and Rientjes (2005). Soil occupation and building locations can be estimated from satellite imagery, see e.g. (Zhang et al., 2007; Salvati et al., 2016; Li et al., 2019), although fine-scale variations remain difficult to identify. Finally, complex urban geometries information can be derived from very HR aerial imagery, e.g. manhole cover locations in (Commandre et al., 2017; Mattheuwsen and Vergauwen, 2020). To calibrate the resulting models, spatially sparse flow observations (e.g. water depth time series from limnigraphs) can be combined with high-water marks (HWM), which are typically either collected shortly after the flood or derived from pictures shared by local authorities and inhabitants. HWM are generally more dense in space and can provide a useful complement to observations at static locations, thanks to information on the spatial distribution of the water levels they carry. Indeed, the hydraulic model calibration issue is difficult to tackle and multi-source distributed measurements are valuable.

The benefits of participative methods for data collection have already been identified by flood alert networks (Douvinet et al., 2017) and HWM are sometimes used for validation e.g. in Hocini et al. (2021), for large rural-urban floodplains modeled at relatively high resolution in steady state, and in Neal et al. (2009), for simplified urban flood models. In Nguyen et al. (2022), satellite-based observations of water extents are used to calibrate 13 parameters including longitudinally distributed friction in the minor bed of the Garonne river modeled with the full 2D SW model Telemac2D (Galland et al., 1991). Validation is carried out against HWM and independent satellite data. A relatively low spatialization of friction into 6 patches is defined and their estimation, which is a low dimensional inverse problem, is tackled using with an EnKF-based approach. For relatively fast fluvial flood dynamics, satellite data may not be available due to satellite sampling and water extent data may contain significant uncertainty preventing fine hydraulic calibration. HWM were used in recent works for hydraulic model calibration in Dasgupta et al. (2022) who use crowd-sourced, heterogeneously distributed HWM of a relatively fast fluvial flood for friction calibration with a sequential algorithm in the non-inertial hydraulic model LISFLOOD-FP (Bates et al., 2013). In urban environments, HWM are especially difficult to compare to model outputs for validation or calibration purposes due to locally complex dynamics. To tackle this issue, Smith et al. (2021) proposes a framework to compare HWM to water depths from hyper-resolution hydrological models for fluvial-urban floods, with ADHydro (Ogden et al., 2015) and WRF-Hydro (Gochis et al., 2018) and mesh elements in the tens of meters. Nevertheless, the calibration of spatially distributed parameters in a full 2D Shallow Water (SW) hydraulic model, enabled by sufficient amount of spatially distributed HWMs and water level time series compared to flow variabilities, remains a difficult calibration problem that requires advanced optimization approaches.

Calibrating spatially distributed effective friction, that is using friction effects for momentum dissipation to compensate uncertainties of 2D SW modeling of complex urban flood flows, remains difficult due to the high potential for spatial and structural equifinality when searching for such a parameter using sparse and uncertain observations of complex signals. Since flow observations are generally sparse compared to the physical scales of interest, addressing this challenging issue generally leads to solving difficult ill-posed inverse problems. The spatialization of friction of a 2D hydraulic model has to be adjusted depending on the physical complexity of the real flow and on modeling errors, but also on the availability and quality of calibration data, to enable sufficient freedom in model response for approaching the data. Furthermore, this issue becomes even more challenging to address when other unknown or uncertain quantities, such as temporal forcings at boundaries, must be estimated as well.

Such difficult inverse problems, aiming the estimation of large parameters of different nature, can be adequately solved using Variational Data Assimilation (VDA) methods applied to hydraulic modeling which have proven their capability to infer high-dimensional parameter vectors of such a linear dynamic flow model. Examples of VDA applications to SW models are (Hostache et al., 2010; Monnier et al., 2016) on 2D rural floodplain flows, Pujol et al.

(2020) on large 1D model with multiple inflows, and Pujol et al. (2022) on multi-D floodplain and river network model. Pujol et al. (2022) in particular exploits the informative richness of heterogeneous and uncertain observation sets. In those studies, VDA approaches, based on differentiable hydraulic models, enable to tackle high-dimensional inverse problems associated with increasing friction spatialization. As of yet, no VDA framework was studied for the specific needs of urban floods, i.e. for the optimization of high-dimensional spatio-temporal parameter vectors (uncertain friction and inflows for instance) in 2D hydraulic models with complex street networks, especially using HWMs.

The sparsity of flow observations also encourages the leveraging of multi-source observations, which may be crucial for putting hydraulic models in coherence with our best, yet still incomplete, observation of reality. This requires the use of adequate observation operators, to allow a pertinent comparison of observed data to model states (e.g. as discussed for hydrological models in Smith et al. (2021), for 1D modeling in Pujol et al. (2020) or for 2D hydraulic modeling in (Hostache et al., 2010; Monnier et al., 2016; Pujol et al., 2022)). It also requires sufficient model controllability, i.e. the ability to provide sufficient flexibility to the model response through freedom granted to its tunable parameters to match multi-source distributed observations of rapidly varied hydraulic signals. Therefore, a 2D hydraulic model with VDA capabilities (e.g. DassFlow2D with automatic adjoint derivation Monnier et al. (2016)) is well suited for tackling the simultaneous estimation of large and multi-variate spatio-temporal parameters, such as spatially distributed parameters, e.g. friction, and spatially distributed inflow time series. Furthermore, this property of the VDA method is especially pertinent for urban model calibration, where potentially sharp spatial variations of model parameters may be responsible for important flow variabilities. This creates a specific need in urban models for the inference of high-dimensional spatial parameter fields.at are expected to be partial, heterogeneous and uncertain.

Simultaneously inferring parameters that have correlated influence on model response and observable signatures, however, leads to equifinality issues (Larnier et al., 2021; Pujol et al., 2020). We can distinguish between structural and spatial equifinality. Structural (resp. spatial) equifinality arises when two distinct parameters (resp. different spatial patterns of a given parameter) can lead to similar observed (not fully) model responses within a range of meaningful model parameterizations. Structural equifinality is expected, for example, when simultaneously estimating bathymetry and friction parameters embedded in a friction term from water level observations (Garambois and Monnier, 2015; Larnier et al., 2021). Spatial equifinality corresponds, for example, to a case of two friction parameters fields leading to similar model fit of model response to the available information, e.g. in 1D (Garambois et al., 2020; Pujol et al., 2020) and 2D Fabio et al. (2010) models. Equifinality is a key issue to address for urban flood model optimization, but regularization strategies and constraints are required to enable meaningful estimation of the sought parameters. The use of friction patches (Hostache et al., 2010; Monnier et al., 2016), consisting in spatial clustering of friction parameters to provide a constraint in the forward model, enables to adjust model flexibility and controllability. Using

gradient-based sensitivity maps obtained with an adjoint of a 2D hydraulic model Monnier et al. (2016) to compute Derivative-Based Sensitivity Measures (DGSM, Sobol' and Kucherenko (2009)) to guide the spatialization of model parameters has seldom been done and is studied here.

This study presents the application of a VDA framework (DassFlow2D, Monnier et al. (2016)) for the inference of multivariate spatio-temporal and potentially large parameter vectors by assimilation of multi-source and heterogeneous observations into a 2D full SW model, tested here on a complex urban flash flood case. It focuses on the inference of a boundary inflow hydrograph and spatially distributed friction coefficients performed by assimilation of heterogeneous water depth observations, including HWM and water level time series, and of flow velocity observations. Furthermore, it applies a gradient-based method for the generation of HR sensitivity maps, based on (Sobol' and Kucherenko, 2009; Lamboni et al., 2013). Therefore, the contribution of the study is a demonstration of the potential of a VDA algorithm and gradient-based sensitivity analysis to develop an understanding of the fine structure of spatialized parametric sensitivities and the associated useful power for diagnostic and for recovering complex hydraulic parameters. Particular attention is paid to definition of model degrees of freedom through the definition of friction spatialization, hence of the parameters sought by VDA.

The article is organized as follows. In Section 2, the hydraulic model, the VDA algorithm and the method for gradient-based sensitivity analysis are presented. In Section 3, the study area, the data for the considered flooding event and the model building approach are detailed. In Section 4, a series of gradient-based analyses and inference results are discussed, including the simultaneous calibration of distributed friction patches and inflow hydrograph. The study is concluded in Section 5.

2. Numerical tools and models

This work uses an accurate 2D SW solver implemented in the DassFlow2D[1] hydraulic-hydrological modeling and data assimilation platform. It consists of a Fortran kernel interfaced with Python. A numerical adjoint model, obtained by source to source differentiation of the Fortran core performed with TAPENADE engine (Hascoet and Pascual, 2013), enables access to gradient-based methods for sensitivity analysis and parameter inference. The code is open-source and available through GitHub[2].

2.1. 2D hydraulic model

We consider a 2D spatial domain $\Omega \subset \mathbb{R}^2$ over which the numerical solver is applied and denote by $t \in]0, T]$ the physical time. T is the simulation time period length. The 2D SW equations in their conservative form write as follows:

[1] https://www.math.univ-toulouse.fr/DassFlow/index.html
[2] https://github.com/DassHydro/dassflow2d

$$\frac{\partial}{\partial t}\mathbf{U} + \frac{\partial}{\partial x}\mathbf{F}(\mathbf{U}) + \frac{\partial}{\partial y}\mathbf{G}(\mathbf{U}) = \mathbf{S}_g(\mathbf{U}) + \mathbf{S}_f(\mathbf{U})$$

$$\mathbf{U} = \begin{bmatrix} h \\ hu \\ hv \end{bmatrix}, \ \mathbf{F}(\mathbf{U}) = \begin{bmatrix} hu \\ hu^2 + \frac{gh^2}{2} \\ huv \end{bmatrix}, \ \mathbf{G}(\mathbf{U}) = \begin{bmatrix} hv \\ huv \\ hv^2 + \frac{gh^2}{2} \end{bmatrix}, \tag{1}$$

$$\mathbf{S}_g(\mathbf{U}) = \begin{bmatrix} 0 \\ -gh\nabla b \end{bmatrix}, \ \mathbf{S}_f(\mathbf{U}) = \begin{bmatrix} 0 \\ -g\frac{n^2 \|\mathbf{v}\|}{h^{1/3}}\mathbf{v} \end{bmatrix}$$

with the water depth h [m] and the depth-averaged velocity $\mathbf{v} = (u, v)^T$ $\left[\mathrm{m/s}\right]$ being the flow state variables. The flow model parameters are the gravity magnitude g $\left[\mathrm{m/s^2}\right]$, the bed elevation b [m], and the Manning-Strickler friction coefficient n $\left[\mathrm{s/m^{1/3}}\right]$. $\mathbf{F}(\mathbf{U})$ is the flux of the variable $\mathbf{U}$, $\mathbf{S}_g(\mathbf{U})$ is the gravitational source term, $\mathbf{S}_f(\mathbf{U})$ is the mass and friction source term. Adapted initial and boundary conditions are chosen (see (Monnier et al., 2016; DassFlow, 2019)), namely imposed mass flux at upstream boundary and imposed water depth at downstream boundary.

A well-balanced Godunov finite volume scheme (Godunov and Bohachevsky, 1959) is used to solve Eq.(1). Either a classical first-order scheme with explicit Euler time stepping or a globally second-order Implicit-Explicit (IMEX) scheme with Runge-Kutta time stepping can be used along with a Harten-Lax-van Leer-Contact (HLLC) Riemann solver. This solver is an improvement on the Harten-Lax-van Leer-Contact (HLL) method with a three-wave velocity model for calculating flows (see Toro (2013) for more details).

2.2. Cost function for multi-source DA

Data assimilation aims to optimally combine model and data. It consists in minimizing the discrepancy between model and observations that is measured through a cost function. Let us define a set of heterogeneous observations Y^* and an observation operator $\mathcal{H}$ that converts any component of Y^* into hydraulic model states variables projected into observation space $Y \in \Omega$. * denotes given values. Let us define $\boldsymbol{\theta}$ a control vector of model parameters. It can contain any number of model parameters, including distributed friction and inflow time series as done in this work.

The objective function J is defined as the sum of two terms:

$$J(\boldsymbol{\theta}) = J_{\mathrm{obs}}(\boldsymbol{\theta}) + \alpha J_{\mathrm{reg}}(\boldsymbol{\theta}) \tag{2}$$

where J_{obs} stands for the observation cost function measuring the discrepancy between model and flow observations, and J_{reg} is a regularization term weighted by a coefficient α.

The general form of the observation cost function writes:

$$J_{\text{obs}}(\boldsymbol{\theta}) = \left\| Y(\boldsymbol{\theta}, t) - \mathcal{H}\left(Y^*(t)\right) \right\|^2_{\mathcal{O}_Y} \tag{3}$$

where $\mathcal{O}_Y$ is a covariance matrix defining an euclidean weighted norm such that $\|z\|^2_{\mathcal{O}_Y} = z^T \mathcal{O}_Y z$, with z a real valued vector.

Note that the cost function enables to account for multi-source observations and depends on the sought parameters $\boldsymbol{\theta}$ through the model response Y.

In this work, calibration relies on real and synthetic observations of water depth $h_{\text{obs}}(x, y, t)$ and synthetic observations of flow velocity $\mathbf{v}_{\text{obs}}(x, y, t)$ that are directly comparable to model states through $h(\boldsymbol{\theta}, x, y, t)$ and $\mathbf{v}(\boldsymbol{\theta}, x, y, t)$. For real HWM observations, peak time $\hat{t}_p$ is unknown and must be estimated. Hence the general cost function considered hereafter writes as:

$$J_{\text{obs}}(\boldsymbol{\theta}) = a \left\| h(\boldsymbol{\theta}, t) - h_{\text{obs}}(t) \right\|^2_{\mathcal{O}_h} + b \left\| h\left(\boldsymbol{\theta}, \hat{t}_p\right) - h_{\text{obs}}\left(\hat{t}_p\right) \right\|^2_{\mathcal{O}_{hp}} + c \left\| \mathbf{v}(\boldsymbol{\theta}, t) - \mathbf{v}_{\text{obs}}(t) \right\|^2_{\mathcal{O}_{\mathbf{v}}} \tag{4}$$

where a, b, c are weighting coefficients. The three terms account successively for:

1. the model misfit to water level time series at one or several gauges within the spatial domain, over part or the whole simulation duration, hence a sum in space and time.
2. the model misfit to high water marks at max flooding time $\hat{t}_p$, that has to be estimated if not known.
3. the model misfit to surface velocity observations - in this work we use observations of depth-averaged velocities, hence no observation operator needed.

The purpose of Eq.4 is to provide a single formula for the different cost functions simply used with equal and/or null weights in what follows. Moreover, in the absence of information on measurement errors, the covariance matrices of the observation error $\mathcal{O}_h$, $\mathcal{O}_{hp}$ and $\mathcal{O}_{\mathbf{v}}$ are simply set to the identity matrix.

2.3. Data assimilation problem

The data assimilation problem consists in minimizing the discrepancy between observations and model by adjusting its parameters. Considering the above defined cost function (Eq.(2) and Eq.(4)), the estimation of the parameter vector $\boldsymbol{\theta}$ of the 2D SW model (Eq.(1)) gives rise to an optimization problem that writes as follows:

$$\hat{\boldsymbol{\theta}} = \underset{\boldsymbol{\theta}}{\operatorname{argmin}}\ J(\boldsymbol{\theta}) \tag{5}$$

where $\hat{\theta}$ denotes the optimum parameter vector. This optimization problem is solved using a first order gradient-based algorithm, the classical L-BFGS quasi-Newton algorithm (Zhu et al., 1997). The gradient $\nabla_{\boldsymbol{\theta}} \boldsymbol{J}$ is computed with the help of the adjoint model, obtained by automatic differentiation using Tapenade (Hascoet and Pascual, 2013).

In this work, as affordable with the considered observations, the full control vector $\boldsymbol{\theta}$ can contain spatially distributed friction coefficients n and inflow hydrographs Q_{in} such that:

$$\boldsymbol{\theta} = \left(n\left(x, y\right), Q\left(t\right)\right)^T, \ \forall [x, y] \in \Omega, t \in [0, T] \tag{6}$$

This multi-variate vector of spatio-temporal parameters of the 2D hydraulic model is optimized in order to reduce the misfit between simulated flows and heterogeneous observations of complex 2D urban flows. The optimization is started from a first guess $\boldsymbol{\theta}^*$ on the sought parameters, * denotes here the prior that is given as the flow observation.

Note that the inference capability depends on the informative content of observations and of their spatio-temporal sampling. The inference is particularly challenging in the case of parameters having correlated influence on observations. This is the case, for example, with spatially distributed friction fields, where distinct localised variations can trigger indistinguishable flow signatures, depending on the flow conditions; this relates to spatial equifinality. The simultaneous estimation of such a spatialized friction parameter and another parameter, such as a time-varying inflow hydrograph, makes the inverse problem even more difficult.

2.4. Gradient-based global sensitivity analysis

In the context of difficult inverse problems, analysis of the sensitivity of the model response to its parameters can provide useful guidance, especially if spatio-temporal sensitivity patterns are available. A strength of our differentiable numerical modelling approach is to enable the computation of accurate cost gradients $\nabla_{\boldsymbol{\theta}} \boldsymbol{J}$ with respect to spatio-temporal parameters (see Monnier et al. (2016)).

When dealing with heterogeneous data and structural and spatial equifinality problems, these local sensitivity maps are precious information for determining parameter patches as well as for examining global sensitivities over a plausible parameter space.

The estimation of global variance-based importance measures of model input parameters, called Sobol' indices Sobol' (2001), can be performed with Derivative-based Global Sensitivity Measures (DGSM) as proposed by Sobol' and Kucherenko (2009) (see also Lamboni et al. (2013)).

First and total order indices write Saltelli et al. (2008) $S_i = \frac{V_i}{V}$ and $S_{Ti} = 1 - \frac{V_{\sim i}}{V}$, where $V_i = V\left(E\left[J|\theta_i\right]\right)$ is the variance caused by the input factor θ_i, and $V_{\sim i}$ is the variance of the expectation of $\boldsymbol{J}$ conditional on $\theta_{\sim i}$, i.e. all the variables except θ_i.

Assuming that $J(\theta_1, ..., \theta_N)$ is square integrable over the parameter hypercube $\mathcal{H}^N$, following the Morris importance measure (Morris, 1991; Saltelli et al., 2008), the DGSM proposed by Sobol' and Kucherenko (2009) writes:

$$\mu_i = \int_{\mathcal{H}^N} \left(\frac{\partial J}{\partial \theta_i} \right)^2 \mathrm{d}x \tag{7}$$

This gradient-based measure can be related to total order Sobol' indexes as shown in Sobol' and Kucherenko (2009) through the inequality $S_{Ti}\ V(J(\theta)) \leq \mu_i$. Then it can be extended to normal and uniform measures (Lamboni et al. (2013)), such that if input factors are independent and if factor θ_i follows a normal distribution of variance σ_i^2 then:

$$S_{Ti}\ \leq \frac{\mu_i \sigma_i^2}{V(J(\theta))} \tag{8}$$

The components of the gradient $\nabla_{\boldsymbol{\theta}} J\left(\tilde{\boldsymbol{\theta}}\right) = \left(\frac{\partial J(\tilde{\theta})}{\partial \theta_1}, ..., \frac{\partial J(\tilde{\theta})}{\partial \theta_N} \right)$ at a given point $\tilde{\theta} \in \mathcal{H}_N$ can be computed accurately by solving the adjoint model of the forward numerical model presented in section above, even in high dimension which is hardly possible with finite difference approaches.

The computation of DGSM is made as in Chelil et al. (2022), where the global adjoint sensitivity analysis is applied to a spatially lumped hydrological model, considering a uniform sample of each member of $\boldsymbol{\theta}$ as $\theta_i = (a_i - b_i)\epsilon_i + b_i \forall i = 1..N$ with $\epsilon \in u(0,1)$ and $[a_i, b_i]$ the expected range for the parameter θ_i. Then, for each sample $k = 1..K$ of the sampling, the forward 2D SW model is run to compute $J_k(\tilde{\theta})$ and the adjoint model is run to compute $\left(\frac{\partial J(\tilde{\theta})}{\partial \theta_i} \right)_k^2$ and finally get the expectation $E\left[\left(\frac{\partial J}{\partial \tilde{\theta}_i} \right)^2 \right]$ over the sample.

Gradient-based local sensitivity maps obtained by solving a numerical adjoint model are presented in Castaings et al. (2009) for a 2D hydrological model and in Monnier et al. (2016) for a 2D SW model. In this article, in order to study spatial variations in the sensitivity of a spatialized parameter, we present maps of cost function gradients with respect to fully distributed homogeneous friction coefficients. We then compute the expectation $E\left[\left(\frac{\partial J}{\partial \theta_i} \right)^2 \right]$ over a sample of homogeneous friction distribution within the expectable parameter space, i.e. within parameters bounds defined a priori. The goal is to inform the spatialization of the friction parameter to reach appropriate controllability, by sampling sensitivity over the parameter space that can be expected to be visited during the iterative deterministic assimilation process.

Appropriate controllability is intended as a sufficient spatialization of friction into spatial patches, i.e. giving freedom to model parameter, hence to modeled flow variability, such as enabling a better fit to the available observations while maintaining parameters identifiability. In this approach, the control spatialization is guided by analysis of hydrodynamics and data availability, which is originally complemented in this article by the HR sensitivity maps

obtained with DGSM. A parameter control vector is defined so that it can be inferred, which requires that simulated quantities at observation locations are sensitive to control parameters.

3. Study area

The studied catchment is located in Abidjan, capital of the Ivory Coast, a rapidly growing megapole with a tropical climate. It covers part of the Riviera-Palmeraie neighbourhood, which has suffered from recurrent flash flooding during both the high and low rain seasons for over a decade. The area is centered around the channel of the Ministre street that crosses the neighbourhood. Along the Ministre street, an existing asphalt road was washed away by the successive floods. The materiel is packed dirt with regular obstacles such as rock piles, cars (see e.g. Fig.2(b)). Upstream from the study area, the catchment presents two distinct urbanized zones, one of which features a dam just upstream from the model boundary. Flow from both watersheds enters the study area through the Ministre street channel.

A particularly intense 4.5-hour-long flooding event that occurred in 19 june 2018 was documented through limnigraphic measurements from a gauging station located in the Ministre street channel and the collection of HWM throughout the study area (see Fig.3, left). The urban flooding was caused by an upstream flood hydrograph peaking at around 57 m^3/s, according to hydrological model estimates. The impact on local hydraulics of this inflow is recorded at the limnigraphic station, which carries important information on its temporal variations. Distributed information on local dynamics and on the upstream flow is carried by HWM, with depths recorded outside of the channel often reaching 1.5 m (see Fig.1).

HWM were collected the day after the event using a ruler and a GPS. Measurements are consistent overall in terms of spatial variations of water surface elevation, oftentimes showing homogeneous variations along a street. Some variations are less consistent with overall trends, but may be the result of local obstacles. Measurement uncertainty with the ruler is expected to be around 5mm. Compounding errors are linked to i) placement the bottom of the ruler on uneven ground, ii) generation of the LiDAR DEM and iii) projection of LiDAR data on the mesh grid, and difficult to estimate. The data and modeling uncertainties will be classically compensated through friction calibration, with various degrees of spatialization hence freedom.

In this work, taking into account spatio-temporal observations of flow depth, the goal is to estimate (1) an unknown inflow hydrograph and (2) friction patterns of adequate spatialization in a 2D SW model. This hypothesis of 2D hydraulic modeling with a single friction source term to represent dissipation of mechanical flow energy is widely used and enables effective flow modeling of urban floods over complex geometries with local geometrical singularities (e.g. Arrault et al. (2016), Chen et al. (2018)). The use of an optimized friction enables to effectively compensate uncertainties of 2D modeling of complex and multiscale 3D flows over local geometries (see e.g. actual street view in Fig.2(b)).

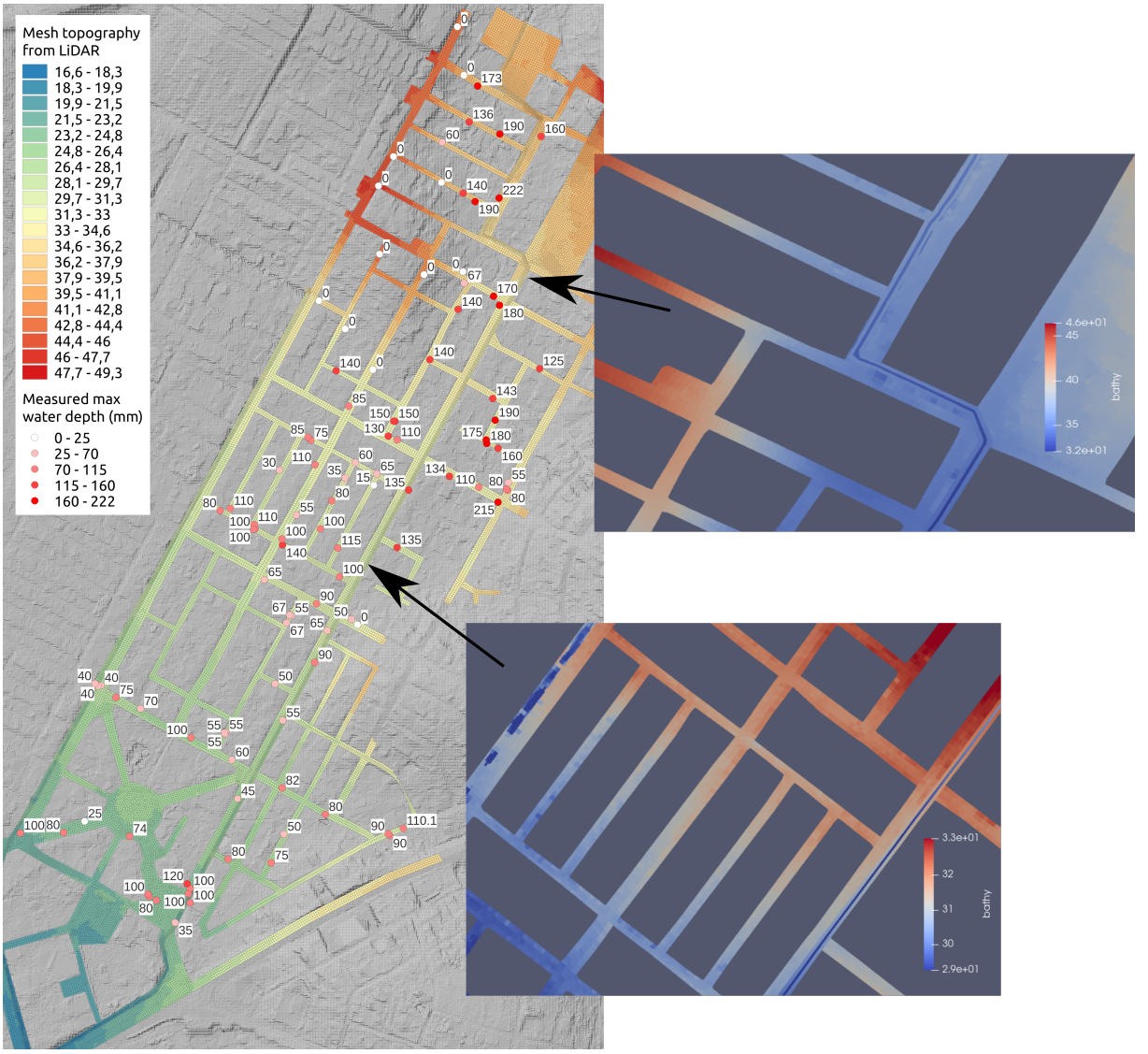

Figure 1: HWM locations with recorded water depth values in mm and model topography plotted on part of the mesh only for clarity. LiDAR DEM in background. HWM are overall spatially consistent with each other and LiDAR bathymetry. Observations of 0m depths are not used in assimilations. Zooms show homogeneous street slopes that are representative of the studied area. Top zoom focuses on the second double bend where overflow occur. Bottom zoom shows a street network of interest (studied in Section 4.1.2). The Ministre channel is visible in zooms and has a depth of 2m and a width of 2m (see Fig.2(a)).

Furthermore, the recent installation of a fixed camera at the gauging station should allow for the generation of surface velocity observation fields in the near future, through numerical velocimetry methods (using tools like e.g. ANDROMEDE (Cassan et al., 2024) or Fudaa-LSPIV (Jodeau et al., 2019)). The anticipated availability of this kind of observations motivates queries into the potential usefulness of surface velocity observations, especially for flooding events.

(a) View of the channel, at the limnigraph location. Posterior to HWM dataset.

(b) Still from news footage on the 2018 flood: the Ministre street after the flood peak. Approximate location of channel edges in red.

Figure 2: Real views within the hydraulic domain

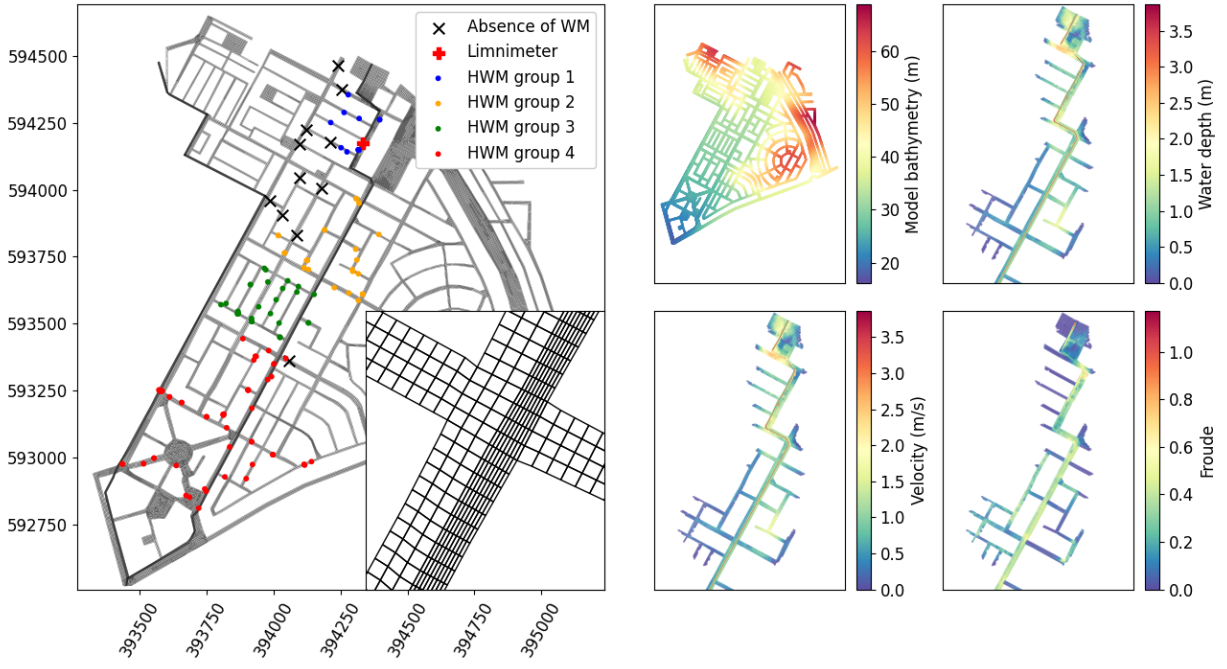

Figure 3: Model results and mesh with observation locations. Left: Full model mesh including zoom around an intersection with the Ministre street, where the mesh is refined around the channel. HWM locations for the flooding event are divided into 5 groups based on their distance from the upstream injection point and their distance from the channel. Modeled values of water depth, flow velocity and Froude are provided at peak flow for a hydrograph of max flow $57\mathrm{m}^3/\mathrm{s}$ and for an homogeneous friction of $n = 0.07\ \mathrm{s/m}^{1/3}$. Average slope of the channel is 0.98%. Average slope of the straight part of the Ministre street is 0.84%.

3.1. Mesh building

The 2D unstructured mesh of the streets is composed of 52k quadrangular elements adapted to the sharp angles of the street network with crossroads and 2D flow patterns. Mesh resolution is designed to allow fast computation, especially useful in inverse modeling, and allow modeling the rapidly varied phenomena we expect around local

geometries. Buildings are assumed impermeable, which is reasonable since most lots around the Ministre street are well delineated by high walls and building entryways are often blocked by smaller walls built in response to recurrent flooding. Model topography is given by a 2.5m LiDAR DEM. Within the channel, homogeneous slopes were manually set based on LiDAR topography analysis: 0.75% on the first 1500 m of channel and 1.05% on the remaining 900 m.

Most cells have an edge length of around 4m, i.e. from 2 to 4 cells per street width. Given the relative smoothness of the topography and the homogeneity of street-scale slope in the model, this appears to be a reasonable trade-off between resolution and computation time. The mesh was refined around the Ministre street channel to accurately model the location and elevation of its bottom and its 2 meters-high side walls (see mesh zoom in Fig.3, the channel has a width of 2m, or 2 fine cells). The time step is adaptive with a Courant-Friedrichs-Lewy (CFL) condition value of 0.8, which results in time steps generally between 0.2 and 0.02 s.

3.2. Direct model setup

Based on field experience and interaction with local inhabitants, the flooding of the street network is largely due to the Ministre street channel overflow that is inflowed by a single upstream hydrograph. This hydrograph is the only considered inflow boundary condition for the 2D SW model resolution.

While other inflow locations are known in the downstream part of the model, forward simulations have shown that these downstream inflows do not influence the hydrodynamic behaviour observed by HWM groups 1, 2 and 3 (see Fig.3, left). They contribute to flood extent in the downstream part of the model only, due to the relatively high slope. Since these inflows are not known a priori and their influence is not observed independently through time series (only through a subset of HWM observations), they would be very difficult to estimate. This is why we choose not to account for them and instead focus on the upstream inflow. This means that the hydraulic control exerted by the downstream BC is not expected to match reality closely and it may be difficult to fit the model to observations in HWM group 4.

Other preliminary simulations showed that the contribution of rain over the urban hydraulic modeling domain to the total volume is low. Homogeneous rain was modeled using rain intensity time series from the nearest pluviometer, injected over the hydraulic domain as mass source term. A runoff coefficient of 1 is assumed. This setup corresponds to what we expect to be the worse case of runoff generation in the area, hence it leads to an estimation of the maximum expected contribution of runoff to the flood. At peak flow, the contribution of rain is under 11% of the water volume in the model. This is why, in an effort to focus on channel overflow and complex flow distribution in the nearby streets, the presented model does not account for rain within the hydraulic domain. It appears feasible to fit most HWM observations by calibrating only the upstream inflow and distributed friction parameters.

4. Results and discussion

The aim of this section is to reconstruct an unknown upstream inflow hydrograph, while calibrating spatially distributed friction of a 2D SW model by VDA of multi-source flow observations. The common focus of the following numerical experiments is the analysis of the impact of the degrees of freedom given to a distributed friction parameter on the assimilation results in a context of spatial equifinality. The method is applied to a single flood event with limited but informative amount of data, hence validation on other events cannot be performed.

The presented cases are of varied complexity in terms of the informative content of the observations used. A summary of considered parameter controls and observations is presented in Table 1.

A homogeneous friction value of $n = 0.07$ s/m$^{1/3}$ was chosen as an initial estimate. It is a relatively high friction in comparison to classical values used in hydraulics such as those in reference tables (e.g. Chow (1959)), especially for the channel, which has smooth concrete bottom and sides, but it leads to fair fits overall (Fig.7, red). This homogeneous friction distribution is used as a target value around which local gradients are sampled for sensitivity maps, in Section 4.1, and as a prior value in assimilation experiments, in Sections 4.2 and 4.3.

In Section 4.1, distributed friction is given a high degree of freedom, in the context of sparse (Section 4.1.1) and dense (Section 4.1.2) observations. Spatial equifinality is discussed using gradient-based sensitivity metrics, highlighting the complexity of the flow in the street network as seen through the assimilation process.

In Section 4.2, distributed friction is given a lesser degree of freedom with the intent to infer inflow hydrograph and friction simultaneously. Real observations, spatially sparse with regard to the hydrodynamic phenomena at play, but including a water level time series relevant to infer the time varied inflow, are assimilated.

In Section 4.3, distributed friction is given a high degree of freedom in a twin experiment setup, in the context of sparse, local observations of localized phenomena. High friction areas are used to generate synthetic observations of complex behaviours, then friction is inferred from these observations starting from a homogeneous prior.

For all experiments, the regularization weight is set to $\alpha = 0$. The only applied regularizing effect is achieved through parameter spatialization in the direct model.

4.1. Gradient-based sensitivity maps: expectable optimization trends and hydraulic controls spatialization

The local gradient of a cost function with regard to a set of chosen model parameters, $\nabla_{\theta} J(\tilde{\theta})$, can provide an interesting insight into model sensitivity, locally at a given point $\tilde{\theta}$ in the parameter space $\mathcal{H}^N$. Furthermore, our differentiable hydraulic model enables computation of accurate HR gradient maps for high-dimensional parameter vectors by adjoint model resolution. As proposed in Section 2.4, the information conveyed by several local gradient maps can be combined to compute, for a given sample of the parameter space, global sensitivity in the form of spatial

Section	Content	Parameter vector content (total elements)	Considered observations
4.1.1	Local gradient maps	Fully distributed friction (52118)	Synthetic, sparse HWM at peak flow
4.1.2	Global gradient map	Fully distributed friction in area of focus (1208)	Synthetic water depth time series at all cells of area of focus
4.2	Full model calibrations	Distributed friction (2, 15 or 45) and upstream hydrograph (20)	Real HWM and water depth time series at limnigraph
4.3	Localized high-friction calibration	Fully distributed friction (52118)	Synthetic water depth and flow velocity time series at chosen locations

Table 1
Summary of experiment setups performed in Section 4

maps. This subsection presents (i) local gradient maps of distributed friction and (ii) a spatial map of global sensitivity as defined in Eq.(8).

4.1.1. Local friction sensitivity maps

The local gradient maps are generated for a twin experiment. Observations of water depth are generated at the locations of the actual HWM measurements using a reference model. This reference model features a homogeneous friction of $n^* = 0.07$ s/m$^{1/3}$ at all cells and a 3h symmetrical triangular upstream hydrograph of peak flow 30 m^3/s as upstream BC. The distributed gradients of the cost with respect to friction are computed for each cell, for two prior values of spatially homogeneous friction ($n = 0.065$ and $n = 0.075$ s/m$^{1/3}$), as presented in Fig.4.

A positive (red in Fig.4) gradient value at a given cell indicates that the first iteration of our VDA method would likely lead to a decrease in friction at that cell. A negative (blue in Fig.4) gradient would lead to an increase in friction.

An underestimation of the friction's first guess ($n = 0.065$, -7% from the reference n^*) leads to higher sensitivity upstream (Fig.4a). Positive gradients are computed in Area 1, outside of the channel, while gradients are negative in the channel, between two bends. An increase in friction in the channel in this area would exert a stronger hydraulic control at or before the first bend, hence increasing the underestimated depths upstream. Downstream, other positive gradients (Area 2) indicate that depth at observation points in the lateral streets is dependent on local friction, both in and out of the channel. More spatially varied gradients are visible around the observations closest to the channel and around the limnigraph (Area 3).

An overestimation of the friction's first guess ($n = 0.075$, +7% from the reference n^*) causes more outflows toward the street adjacent to the channel, leading to a larger area of interest (Fig.4b). Positive gradient values on most of the channel cells, especially downstream, indicate that the assimilation process should overall appropriately lead to a reduction of friction. Several clusters of contrasted gradient values appear along the channel (e.g. Areas 1 and 2) and at street intersections (e.g. Area 3). This means that a local control impacting the flux distribution at these important intersections can help reduce misfit to HWM observations, even when straying further from the lower

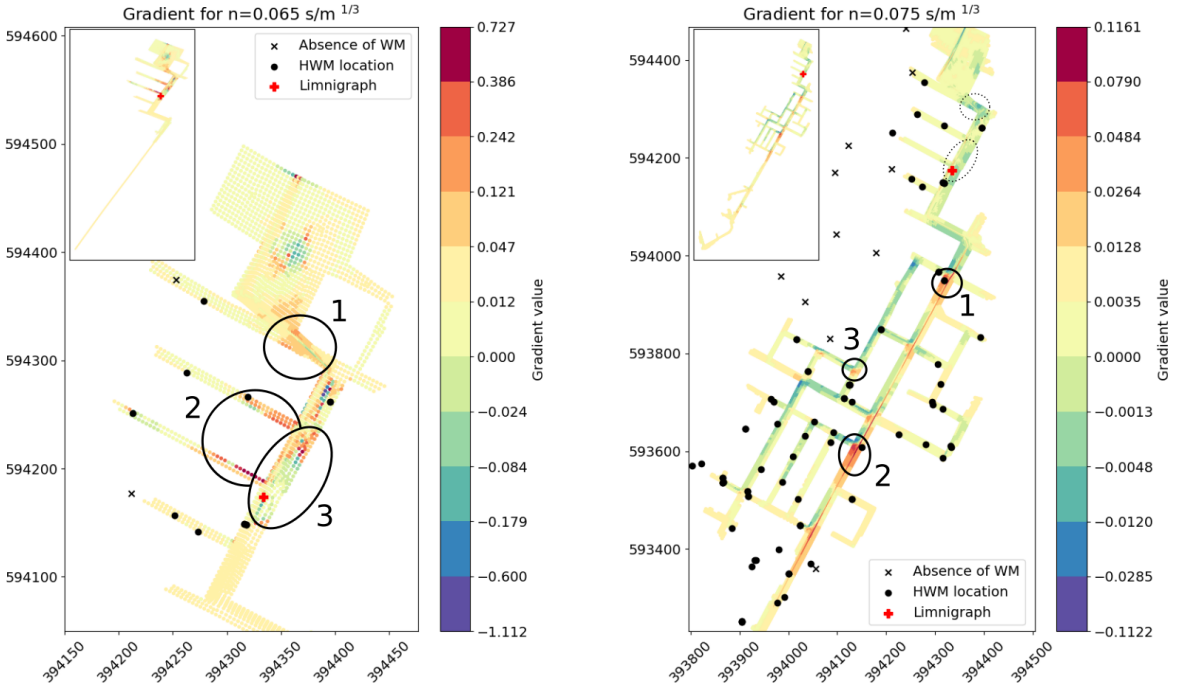

(a) Homogeneous prior: $n = 0.065 \mathrm{s/m}^{1/3}$

(b) Homogeneous prior: $n = 0.075 \mathrm{s/m}^{1/3}$

Figure 4: Maps of observation cost function sensitivity to friction parameter $\frac{\partial J(n)}{\partial n}$, locally in parameter space for $n = 0.065$ or 0.075 $\mathrm{s/m}^{1/3}$. A positive (resp. negative) value means the assimilation process should decrease (resp. increase) the parameter to reduce cost. The reference friction $n^* = 0.07$ $\mathrm{s/m}^{1/3}$ is used to generate observations at HWM locations and cost function is computed with the water depth time series as $J(n) = \left\| h(n,t) - h_{\mathrm{obs}}(n^*,t) \right\|_2^2$. Gradients are computed at all cells of Ω. Null values of gradient are not plotted. Left: gradient maps for $n = 0.065$. An underestimation of friction leads to a decreased flooded area, mostly limited to around the limnigraph. Right: gradient maps for $n = 0.075$. An overestimation of friction leads to an increased flooded area in the street network. The top-left miniatures present computed non-zero gradient values over the whole hydraulic domain.

reference homogeneous friction. Indeed, a reduction of the cost may be achieved "for wrong reasons" by rerouting water to areas where it has less impact on the cost functions, i.e. "hiding" water from the assimilation process in un-/less-observed or insensitive areas.

These gradient maps are those used in the iterative data assimilation process. The sign of the gradients indicates by definition the rate of variation of the functional J with respect to parameters, i.e. the descent trend in parameter space, so positive gradient means that reduction of the cost would be obtained by an decrease of this parameter locally in the hydraulic domain, and conversely. They show that parametric sensitivity in our street network is complex even with spatio-temporally dense observations from a homogeneous reference model and starting from homogeneous priors. The trajectories that they indicate provide some insight into the expectable optimization trends and inferred spatial patterns of parameters given high degrees of freedom. Still, they may not tell the whole story. Indeed, emerging hydraulic behaviors in subsequent parameter optimization iterations, such as a different channel overflow location or a different

flow repartition within the street network, may lead to different spatial distribution and relative weights of the gradient. Hence the need to propose global sensitivity evaluations that sample a number of expectable hydraulic behaviours and inform on its spatial distribution across all iterations, in order to adapt parameter spatialization.

4.1.2. Global friction sensitivity maps

A new setup is defined to study the global sensitivity of cost to distributed friction in a limited area of the hydraulic domain: a subdivision of the flooded street network. The spatial domain is restricted to limit computation costs. Flows reach the considered area from multiple directions, having seen potentially complex mixing upstream, hence inflows to the considered area are highly dependent on friction as well as peak upstream inflow.

Observations of water depth are generated for each cell of the considered hydraulic subdomain of 1402 cells (see Fig.5) throughout the simulated period, The reference model has a homogeneous friction of 0.07 $s/m^{1/3}$ and is inflowed a 1.5h symmetrical triangular hydrograph of peak flow 54 m^3/s. Peak inflow is higher than in Section 4.1.1 to ensure the area of interest is flooded for all below friction values.

A series of local gradient maps are generated for two separate triangular hydrographs and for 7 homogeneous friction values. The peak flow values of these hydrographs are $Q_1 = 50$ and $Q_2 = 60$ m^3/s. The friction is given by a uniform sampling of the range of expectable values: $n_i = (a - b)\epsilon + a \ \forall i = 1..7$, with $a = 0.04$, $b = 0.1$ and $\epsilon = 0.01$. Q_2 generally leads to earlier channel outflows than Q_1 and friction values also influence propagation times in the streets and channel. This complexity is observed downstream, in a street network that receives inflow from both local overflows and upstream urban areas.

Global gradient maps are generated for each inflow hydrograph (see Fig.5). Local gradients are available in Fig. 10 in the Appendix. They aim to identify sensitive areas across the range of friction that the assimilation may cover during its iterative process.

The global maps further underline the role of localized friction in the control of flow at intersections in the street network. Sensitivities are higher with an upstream peak inflow of 60 m^3/s (Fig.5, right) which simply reflects that this setup is further away from the target model than the 50 m^3/s peak flow on, hence higher cost and gradient values. Relative sensitivity values at hotspots vary but their location remains the close to the same. This can be explain by the spatial variation of the observed misfit. With a $60m^3/s$ peak flow, higher sensitivity is computed to the east, i.e. close to the overflowing drain and before this excess flow can be distributed in the street network, hence a higher modeled water depth misfit. With a lower peak flow of $50m^3/s$, the misfit near the channel is lesser, hence a different relative distribution of sensitivity and a relatively higher sensitivity far from the channel. Overall, both maps lead to the identification of similar sensitivity patterns, regardless of the considered inflow. This seems to indicate that the

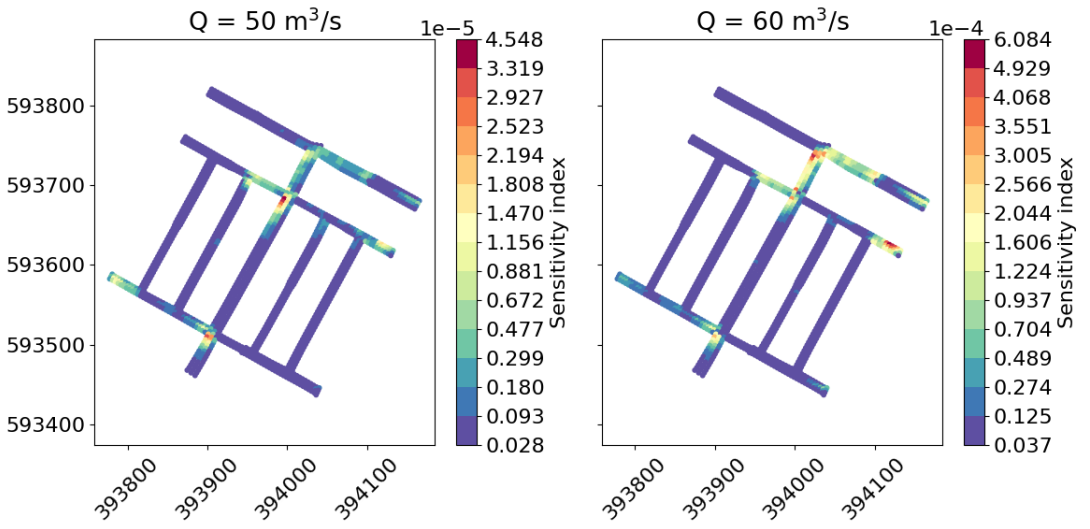

Figure 5: Global sensitivity maps of $E\left[\left(\frac{\partial J(\theta)}{\partial \theta_i}\right)^2\right]$ for 7 samples of expectable homogeneous friction ($0.04, 0.05, 0.06, 0.07, 0.08, 0.09, 0.1$ m/s$^{1/3}$) for two synthetic hydrographs with respective peak flows of 50 m^3/s (left) and 60 m^3/s (right). Local gradient maps of the parameter space samples are plotted in Appendix A.

simultaneous inference of a time-dependent inflow hydrograph and of distributed friction should not lead to a large difference in inferred friction patterns.

More generally, across the sampled parameter space, there is a risk for spatial equifinality in the context of sparse observations of complex phenomena. The above sensitivity maps provide insight on the spatial location of areas sensitive to the sought parameters, hence on where the assimilation method could lead to parameter corrections, which pertains to model controllability.

A fully distributed friction parameter would enable a higher controllability of model response, by enabling local corrections and the creation of variabilities in the simulated flow. Assuming that the reality is indeed varied, it may allow to better fit observations. Nevertheless, it is obvious that spatially dense observations are needed to constrain a spatialized parameter while avoiding spatial equifinality. Inversely, a uniform friction is easily identifiable from few observations, but it does not give enough controllability to fit spatialized observations like those available in our study area. The sensitivity maps help reach a sensible middle ground for the friction spatialization, with appropriate degrees of freedom, where spatial parameters patches are defined in coherence with available observations, sensitive areas and a priori knowledge of realistic parameter distribution.

4.2. Model calibration from available data

Building on sensitivity analysis, we devise a strategy where appropriate controls are defined in the form of friction patches that enable model flexibility while avoiding spatial over-parameterization for the simultaneous inference of friction and upstream inflow.

4.2.1. Upstream inflow inference

The observation most informative about the upstream discharge is the water depth time series obtained at the limnigraph. It is located upstream (Fig.3) of most expected channel overflows.

In a first assimilation setup, we attempt to estimate the upstream inflow $Q_{in}(t)$ from available observations at the limnigraph only. While peak flow estimates from hydrological modeling were available, the shape of the hydrograph was not known. This is why we chose to infer this uncertain parameter as enabled by our assimilation framework, showcasing the value of water level time series inside the hydraulic domain even without using a priori peak flow knowledge from the hydrological model.

We set an homogeneous value of friction $n = 0.07\ \mathrm{s/m^{1/3}}$ and we choose a constant discharge of $5\ \mathrm{m^3/s}$ as a prior value for $Q_{in}(t)$. This arbitrary constant low flow value does not create channel overflow and carries no information on discharge amplitude or temporality, hence any such inferred variability will be extracted only from the limnigraphic observation.

From this limited information and no a priori knowledge on hydrograph shape, a complex hydrograph shape is inferred. Its peak flow is $44\mathrm{m^3/s}$, quite close to the estimated $57\mathrm{m^3/s}$ when considering the prior value of $5\mathrm{m^3/s}$. The hydrograph and its corresponding water surface elevation at the observation site are represented in Fig.6. In what follows, the simultaneous inference of upstream hydrograph and friction fields is possible thanks to considering spatially distributed HWMs in addition to the water level time series at one location. The current inferred hydrograph serves as a prior for subsequent inference setups, where inferred peak inflows reach $58\mathrm{m^3/s}$ with increased performance at the limnigraph (see Fig.7, top right).

4.2.2. Simultaneous inference of distributed friction and upstream inflow

Leveraging both limnigraph and HWM data could allow the calibration of both inflows and distributed parameters. However, as underlined in the previous sections, the distribution of spatial parameters should be coherent with both observations and modeled hydraulic behaviours. In the following, we attempt to simultaneously infer the upstream hydrograph, with a prior value set from a previous inference, and spatialized friction, with a prior homogeneous friction of $n = 0.07\ \mathrm{s/m^{1/3}}$, in setups of increasing complexity regarding the number of spatial patches. Performance of the prior and calibrated models is presented at HWM and at the limnigraph in Fig.7.

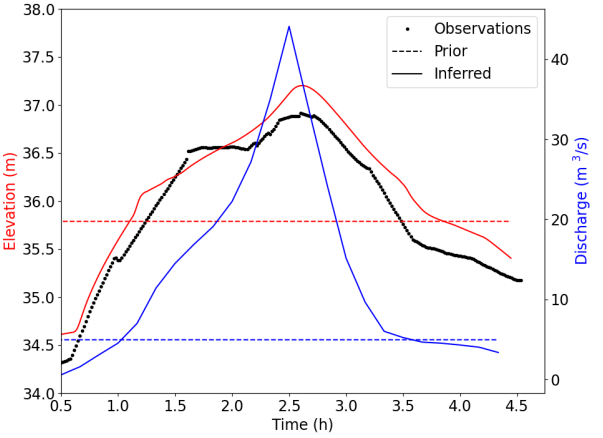

Figure 6: Inference of inflow time series from limnigraph observations starting from an flat prior ($5 m^3/s$).

For HWM observations, the time of maximum depth $\hat{t_p}$ is estimated for each HWM from a direct simulation using the prior values for inflows and friction. It is not updated during the assimilation process. Indeed, the emphasis is put on the VDA capacity to infer spatio-temporal parameters of a 2D SW model (friction and inflow discharge) from heterogeneous distributed observations (HWMs and water level time series), with simplified hypothesis regarding data uncertainties. Uncertainty on maximum water depth time is around 20min based on numerical experiments. It is controlled at first order by the inflow hydrograph and also by channel overflow location and timing, hence by friction effects.

- FrictionSet1 is the simplest setup, based on simple a priori knowledge only. We define two patches: the first containing all cells within the channel, and the second containing all other cells, i.e. street cells. This

- FrictionSet2 leaves some degrees of freedom to the model in the street network, but the patches are much larger than identified sensitivity hot-spots. We define 15 patches (see inference results in Fig.8, left). One patch contains cells within the channel, and the other patches contain subdivisions of the street cells where flooding is observed. This experiment A key assumption of this set is that the inference of friction requires more controllability outside of the channel than within.

- FrictionSet3 gives the model more flexibility within the channel, which could help change where overflows toward the street network occur. We define 45 patches (see inference results in Fig.8, right). In the street network, patches span either one large street or a group of smaller streets within the flooded area. Around the channel, in the Ministre street, one patch is defined between each intersection with another street.

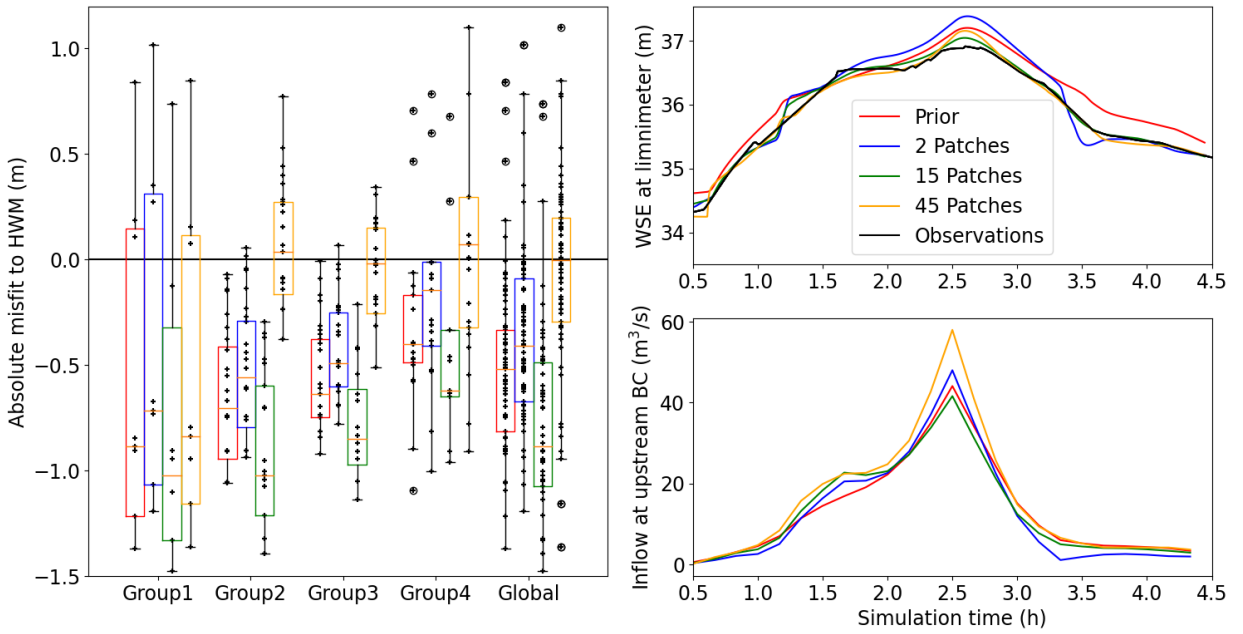

Figure 7: Model performance at HWM and at the limnigraph for FrictionSet 1, 2 and 3, after simultaneous calibration of upstream discharge and distributed friction coefficients, and for their common prior. Left: absolute misfit to observed water depth at HWM locations. Each individual misfit is plotted as a black cross, outliers are denoted by a black cross with a circle. HWM groups are defined in Fig.3. Top right: Simulated water surface elevation at the limnigraph. Bottom right: mass flux injected at the upstream boundary.

The simple FrictionSet1 affords very little controllability to the inverse problem. Calibration of the two patches leads to friction values of 0.059 $s/m^{1/3}$ in the channel and 0.045 $s/m^{1/3}$ in the streets. High friction in the channel helps cause overflows, but water depth in the street network are still underestimated. At around 3.5 hours, a sharp change in modeled water depth at the limnigraph (Fig.7, top right, in blue) reflects how a slight change in upstream inflow (which is around $5m^3/s$ at 3.5h) can impact resulting water depth, thus the quadratic cost function. It features a reasonable improvement of the overall fit to observations in all 4 HWM observation groups.

In FrictionSet2 however, the result of the calibration process is an overall degradation of the fit to HWM observations, while a improved] fit is obtained at the limnigraph (Fig.7, in green). Although FrictionSet2 leads to a lower cost function than the prior, misfit is reduced at the limnigraph but increased at HWMs. Remember that the absolute misfit plotted in Fig.7 is not the cost seen by the assimilation process. This result can be explained by a spatialization of friction ill-adapted to the phenomena that lead to street flooding. The model is given flexibility upstream, around the limnigraph, but not along the Ministre street, where local overflows are expected. This leads to a reduction of uncertainty only in the upstream part of the model, where the parameter spatialization allows such improvement, at the expense of the accurate modeling of downstream overflows. Overflows occur at both upstream double bends due to geometry. High friction at the second double bend, outside of the channel, exerts upstream control

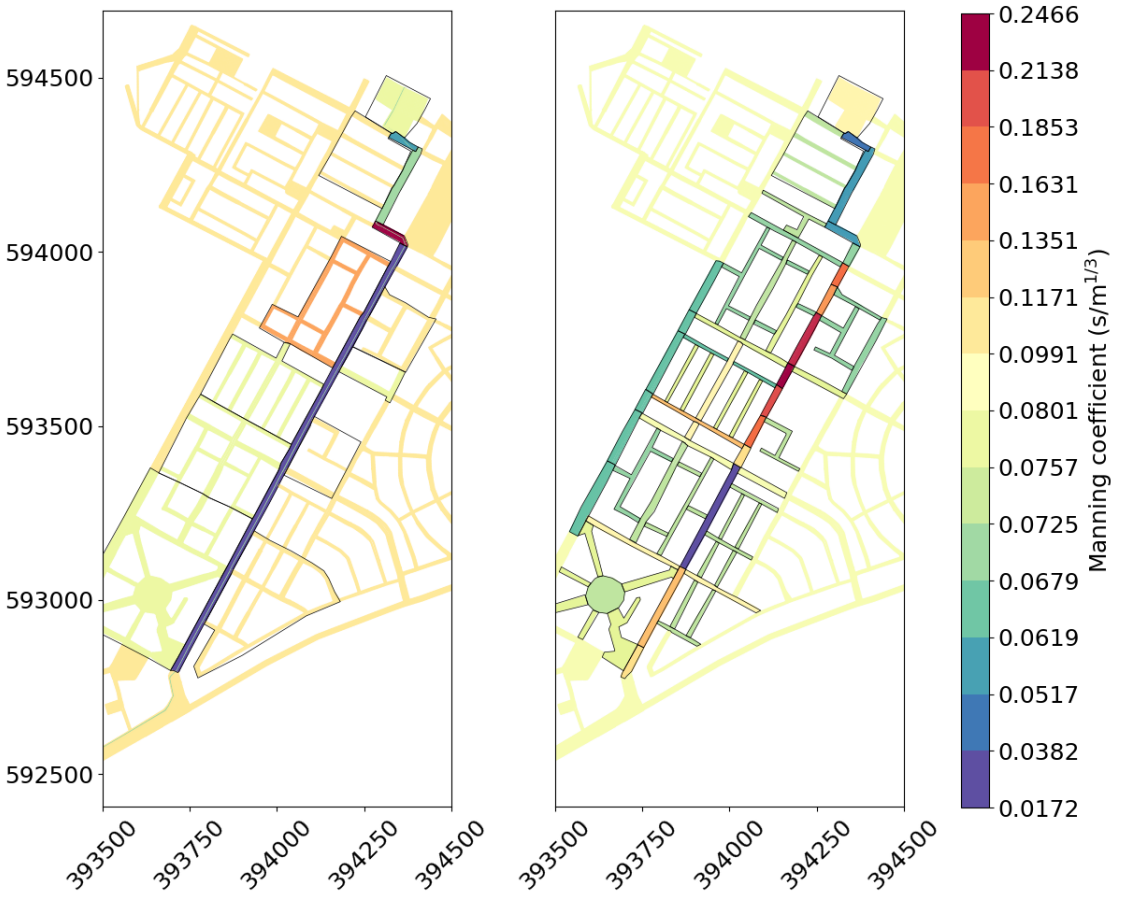

Figure 8: Calibrated Manning friction values for the FrictionSet2 and FrictionSet3 setups. Friction patches are represented as black polygons. The colormap is not linear, friction values are grouped based on a "natural breaks" classification. This enables showing the fine spatial contrasts, or lack thereof, of inferred frictions.

and helps fit HWM group 1 that are within range of the local hydraulic control. This setup, juxtaposed with the simpler FrictionSet1, serves to highlight the need for well-defined degrees of freedom.

FrictionSet3 provides more controllability and leads to greatly improved performance at HWM sites and at the limnigraph (Fig.7, in orange). On one hand, in most of the street network, friction values within a reasonable physical range of 0.06 to 0.09 are inferred. On the other hand, high friction values along the Ministre street allow the model to change the location and intensity of channel overflows. Median water depth misfits in HWM groups 2, 3 and 4 are close to 0, while misfits over HWM group 1 are close to that of FrictionSet1. Adequate degrees of freedom have led the assimilation process to an optimal solution that is a fair improvement over the prior value and features reasonable parameter ranges.

In FrictionSet 2 and 3, quite high (resp. low) friction values – $n > 0.1$ (resp. $n < 0.01$) – are inferred in patches along the Ministre street. They create local overflows toward the street network or instead facilitate the flow along the Ministre street. This enables controlling flow repartition and fitting flow observations by introducing an effective compensation

of modeling uncertainties of urban flood flows over local complex geometries. Excessive upstream overflows may be compensated by low friction values further downstream.

In the end, FrictionSet3 has a good performance for a urban flow modeling with highly energetic flows and complex flow repartition: the median misfit is close to 0m, 50% of stations have misfit between 0.19 and -0.29m and only 13 out of 97 stations have a misfit greater than 0.5m. This is in line with other studies using HWM for validation. In Hocini et al. (2021), misfit to HWM reaches 2m in a model of a river network, with 70% of misfit within the -0.9 to 0.7m range. Neal et al. (2009) models a relatively slow river flood in an urban environment and features misfit to observed water levels as high as 1.5m in an urban model, with most misfit within the -0.5 to 0.5m range. Finally, in Nguyen et al. (2022), no statistical analysis is presented but the validation of the calibrated Garonne model against HWM yields several misfits of more than 1m in absolute value.

Through 3 setups of increasing complexity, we showcased the capability of our VDA toolchain to infer high-dimensional multi-variate control vectors from multi-source heterogeneous observations of hydraulic variables. The studied urban flood has a relative lack of data compared to literature cases with very dense sensors networks and rainfall radar for instance, but the available LiDAR topography plus a water depth time series and HWMs already provide very interesting information as shown by our results. We underlined the usefulness of the method for cases with limited flow observations and the necessity for adequate friction parameter spatialization, which is based on hydraulic knowledge and sensitivity analysis.

4.3. Assimilation of local controls from multi-source heterogeneous observations

Regarding local singularities, this section takes a closer look at the capability of the assimilation process to infer distributed parameters with localized influences on flow. It focuses on the inference of two strong local hydraulic controls and the challenge of correctly attributing their spatial signatures from multi-source observations in a global optimization setup in space and time (see cost function in Eq.(2)). The below inverse problem is purposefully over-parameterized in order to both underline the capability of the assimilation process to handle high-dimensional controls and showcase spatial equifinality at a finer scale.

A new synthetic reality was generated to include two small areas of high-friction ($n = 0.2$ s/m$^{1/3}$) that exert upstream hydraulic controls. The first area is located within the channel (Fig.9, middle, blue area) and increases outflows from the channel towards the street network. The second is located at a street intersection where it influences flow repartition (Fig.9, right, blue area). Aside from these 5 cells, the friction is set to 0.07 s/m$^{1/3}$ across the model. The inflow is a symmetrical triangular hydrograph of peak flow 50 m^3/s.

The in-channel site is observed through a synthetic limnigraph upstream from the high-friction area. The crossroad site is observed through modeled velocities at 3 contiguous cells, where an outflow from the crossroad is expected (see Fig.9b). Both observed quantities are sensitive to the influence of the local high-friction patch.

The cost function is $j(\theta) = \frac{1}{3}\left\|\mathbf{v}(\theta,t) - \mathbf{v}_{\text{obs}}(t)\right\|^2 + \left\|h(\theta,t) - h_{\text{obs}}(t)\right\|^2$ and the control vector is the fully distributed friction parameters $\theta = (n_1, .., n_N)$, where N is the total number of cells. Component weights were set to obtain equal contributions of water depth observations and velocity observations at the first iteration. The prior value is an homogeneous friction of 0.07 $\text{s/m}^{1/3}$.

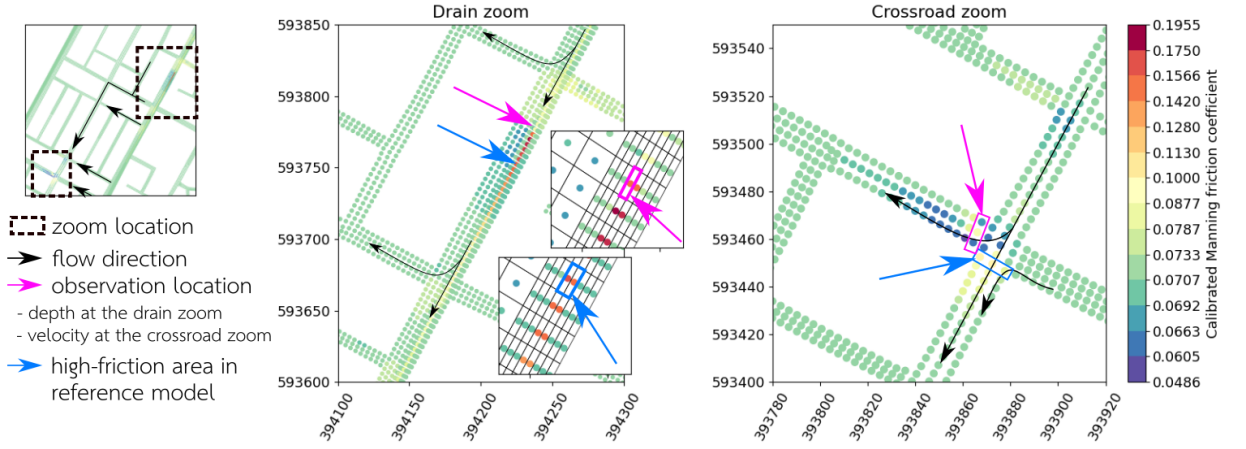

Figure 9: Inferred friction coefficients, starting from a homogeneous prior of $n = 0.07$ $\text{s/m}^{1/3}$, from multi-source observations of a synthetic event. At the channel zoom, an observation of the water depth at a single point is used. At the crossroad zoom, observations of flow velocity at 3 cells are used. High-friction areas near the observations are present in the synthetic reality. Overflows occurring around the channel zoom can reach the crossroad zoom from the north-east. Other overflows from the channel reach the crossroad zoom from the east.

At each site, the inferred spatially distributed friction enables to match the synthetic observations of both types of state variables closely, which is expected in a high controllability twin experiment. However, the area where friction was modified is more spread out in space than the limited high-friction area of the target model.

Around the in-channel high-friction zone (Fig.9, middle), inferred friction is appropriately highest in the channel, with a max value close to 0.2 $\text{s/m}^{1/3}$. However, the longitudinal length of the zone in the channel is overestimated, from 2 in-channel cells in the target setup to around 20 in-channel cells in the inference result. Friction around the channel was incorrectly inferred to be lower than that of the target, further helping the channel overflow in a manner similar to that of the target model from the point of view of the single upstream observation point. Overall, the misfit to water depth observations was attributed, through the assimilation process, to a diffuse high-friction area rather than the very localized zone of the target model.

At the crossroad (Fig.9, right), high friction was attributed to the south-western street, around the location of the target friction patch. A channel of low friction seems to help guide runoff from the northern street to the western street,

reducing the need for high friction at the location of the target high-friction patch. Similarly to the other location, the inferred distributed friction is reflective of the high degree of freedom given to the assimilation process through the use of a HR parameter control vector.

Given the high degree of freedom given to the model, spatial equifinality was expected. Even when we provided no a priori information on high-friction areas locations, we inferred reasonable friction distributions from limited observations. Under the present modeling hypothesis and VDA algorithm setup, the inferred discharge hydrograph and friction patterns are optimal solutions in the sense of the inverse problem solved with available spatio-temporal flow observations.

This inference showcases the capacity of the VDA approach to solve high-dimensional inverse problems by assimilating multi-source data of different types for an urban flood event. It shows that typical observations, i.e. depth from a limnigraph installed in the channel and velocities that can be derived from optic imagery, of the hydraulic controls exerted by localized friction can carry information relative to the location and amplitude of distributed parameters. As for previous inference setups, it is necessary to reach the appropriate controllability to improve inference results.

In an urban context, the calibration of high-friction areas, or other distributed parameters, could be improved by i) the a priori localization of the complex geometries (e.g. through field surveys or satellite imagery analysis), which would allow HR spatialization of parameters and thus appropriate fine scale model controllability and ii) the deliberate collection of flow velocity observation over areas of interest, rather than its area of indirect influence, which would improve identifiability. Such data collection could be carried out with sensors as common and as portable as a smartphone.

5. Conclusion

This article presented a method for the calibration of multi-variate and large control vectors of a 2D hydraulic model from multi-source heterogeneous observations in the context of urban flash floods in complex street networks. A direct-inverse 2D hydraulic modeling toolchain that allows access to gradient-based methods (DassFlow2D Monnier et al. (2016)), was applied in this work. This DA platform was used to study the sensitivity of model states to distributed friction through the generation of gradient-based sensitivity measurement maps and to infer distributed friction and inflow hydrographs from synthetic or real observations, including HWM.

From the obtained results, the following conclusions can be made:

- A gradient-based method for the generation of local and global sensitivity maps was implemented for a 2D SW hydraulic model and applied to an urban flash flood. These sensitivity maps brought insights into the spatial sensitivity of multi-source cost functions to a distributed friction parameter. They show fine scale sensitivity

pattern variations in the street network linked to complex urban flows. They were used, along with hydraulic expertise and flow observations availability, to reach appropriate model controllability through parameter spatialization.

- Spatialized friction parameters and upstream hydrograph time series were inferred simultaneously from real, sparse and heterogeneously distributed observations of flow. When adequate degrees of freedom were granted to the forward hydraulic model through the spatial pattern of distributed friction, misfits to the observed reality were reduced through the assimilation process and the inferred parameters remained within reasonable ranges given the complexity of the modeled hydraulic behaviours, without further constraints of the inverse problem. Overall, the reduction of misfit to flow observations obtained by optimizing friction and/or hydrograph shows the pertinence of the control setups and inverse algorithm.

- Notably, the upstream inflow hydrograph was inferred assuming no prior knowledge of its amplitude or temporality, through the leveraging of a single water depth time series. The inferred peak discharge was consistent with hydrological model estimates.

- Investigations into the capability of the assimilation method to locate and estimate localized high-friction areas from multi-source observations including synthetic velocity fields were carried out. They highlighted the potential use of such local observation fields for the calibration of distributed parameters in complex urban networks. It was shown that local hydraulic signature caused by local loss of mechanical flow energy can carry information on location and parameter value and be used to infer head loss law parameters.

- Finally, the assimilation of HWM along with multi-source limnigraphic observations was successfully carried out for the first time in a variational framework in this paper and enabled the inference of meaningful parameter patterns and values. Assimilation methods could be refined to account for observation and model uncertainty for HWM, including estimations of local maximum depth times, but also for other types of observed quantities acquired through different means.

The experiments presented herein address the issue of degrees of freedom and the framework offers useful diagnostic power for spatial sensitivities structures and optimal combination of 2D hydraulic model and heterogeneous data over complex cases. The presented VDA method was shown to be capable of ingesting multi-source heterogeneous flow measurement in a complex urban flood case, and would enable to consider even more heterogeneous and rich datasets. Having shown the value of HWMs along with water level time series for 2D shallow water urban flood model

calibration, the VDA method is transposable to other urban flood cases. This VDA method enables to infer high-dimensional parameter vectors, which are multi-variate, such as uncertain spatialized friction and inflows as shown here and would also enable to simultaneously infer uncertain bathymetry.

Further work should focus on the systematic identification of pertinent parameter distributions based on gradient-based sensitivity metrics. The development of methods for the large-scale definition of parameter control vectors would allow the resolution of inverse problems over greater hydraulic domains. In urban geometries, where HR hydrodynamics and flow repartition may be explained by fine spatial variations in model parameters, the adequate definition of high-dimensional large scale parameter controls could pave the way towards hydraulic model calibration over full catchments. The capacity of the VDA method to infer high-dimensional parameter control vectors also opens the way to inferring parameters of more complex flow models accounting for example for other friction/drag laws, porosity, rainfall and infiltration. This would nevertheless require richer dataset but also to implement these new features into the forward model in a differentiable manner as required by automatic adjoint model derivation. The demonstrated capability of the VDA method to infer simultaneously spatial and temporal parameters depends on data availability and could also be applied to a more complex shallow model with other source terms, such as accounting for local rainfall on buildings and partially impervious surfaces, infiltration and mass exchanges with sewers and buildings. Accounting for uncertainties on data and priors within the assimilation framework represents an important and interesting topic for further research on other cases and also richer datasets.

A. Appendix: Local gradient maps

A synthetic reality is created. It has a homogeneous friction of $n = 0.07\ \mathrm{s/m^{1/3}}$ and is inflowed by a 1.5h symmetrical triangular hydrograph of peak flow $54\ \mathrm{m^3/s}$. Water depth observation time series are generated at all cells plotted in Fig.10.

The expectable parameter space is sampled for N homogeneous friction values over the whole model. For each sample, a gradient-based sensitivity map is computed (Fig.10). The combination of these maps using the method described in Section 2.4 gives a global sensitivity index over the range of values the VDA process is expected to iterate.

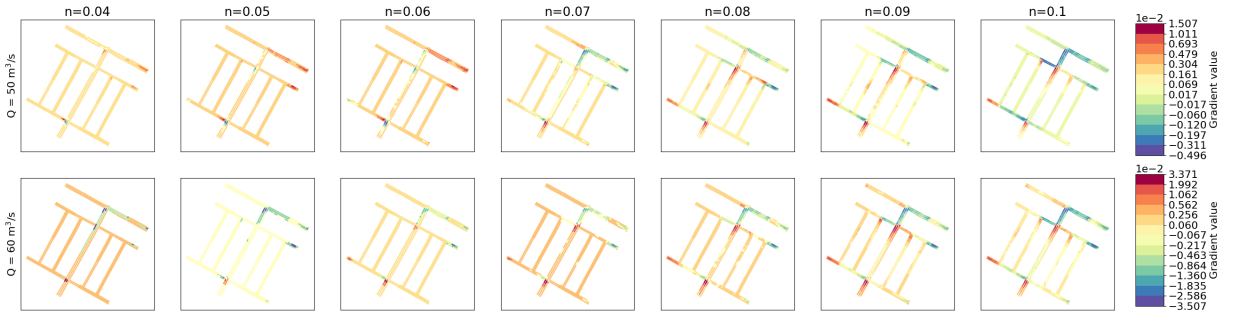

Figure 10: Local sensitivity maps used to build the global sensitivity maps in Fig.5. n (columns) is the homogeneous friction coefficient, Q (rows) is the peak flow of the 2-hour-long symmetrical triangular inflow hydrograph.

Code availability

The DassFlow2D code is open-source and available at https://github.com/DassHydro/dassflow2d.

CRediT authorship contribution statement

Léo Pujol: Conceptualization, Methodology, Software, Formal analysis, Writing - Original Draft. **Pierre-André Garambois:** Conceptualization, Methodology, Resources, Writing - Original Draft. **Carole Delenne:** Resources, Writing - Review Editing. **Jean-Louis Perrin:** Writing - Review Editing.

Acknowledgments

This research work was in part supported by the AMRUGE project from the Ministère de l'Enseignement Supérieur et de la Recherche Scientifique de Côte d'Ivoire, by IRD, the French National Research Institute for Sustainable Development and by the UNESCO International Centre ICIREWARD, International Centre for Interdisciplinary Research on Water System Dynamics. The application of this computational science algorithm and study design has been inspired by scientific discussions led in the MUFFINS ANR project, "Multi-scale Flood Forecasting with INnovating Solutions", ANR-21-CE04-0021-01. The authors warmly thank Luc Seguis for the hydrological modeling of the upstream catchment and for his insights on the study area.

References

Arrault, A., Finaud-Guyot, P., Archambeau, P., Bruwier, M., Erpicum, S., Pirotton, M., Dewals, B., 2016. Hydrodynamics of long-duration urban floods: experiments and numerical modelling. Natural Hazards and Earth System Sciences 16, 1413–1429. doi:10.5194/nhess-16-1413-2016.

Bates, P., Trigg, M., Neal, J., Dabrowa, A., 2013. LISFLOOD-FP. User manual. School of Geographical Sciences, University of Bristol. Bristol, UK URL: https://ec-jrc.github.io/lisflood-code/1_introduction_usermanual/.

Bulti, D.T., Abebe, B.G., 2020. A review of flood modeling methods for urban pluvial flood application. Modeling Earth Systems and Environment 6, 1293–1302. doi:10.1007/s40808-020-00803-z.

Cassan, L., Pujol, L., Lonca, P., Guibert, R., Roux, H., Mercier, O., Courret, D., Richard, S., Horgue, P., 2024. ANDROMEDE—A software platform for optical surface velocity measurements. Environmental Modelling & Software 171, 105883. doi:10.1016/j.envsoft.2023.105883.

Castaings, W., Dartus, D., Le Dimet, F.X., Saulnier, G.M., 2009. Sensitivity analysis and parameter estimation for distributed hydrological modeling: potential of variational methods. Hydrology and Earth System Sciences 13, 503–517. doi:10.5194/hess-13-503-2009.

Chelil, S., Oubanas, H., Henine, H., Gejadze, I., Malaterre, P.O., Tournebize, J., 2022. Variational data assimilation to improve subsurface drainage model parameters. Journal of Hydrology 610, 128006. doi:10.1016/j.jhydrol.2022.128006.

Chen, S., Garambois, P.A., Finaud-Guyot, P., Dellinger, G., Mose, R., Terfous, A., Ghenaim, A., 2018. Variance based sensitivity analysis of 1D and 2D hydraulic models: An experimental urban flood case. Environmental Modelling & Software 109, 167–181. doi:10.1016/j.envsoft.2018.08.008.

Chow, V.T., 1959. Open-channel hydraulics: New york. US Army Corps of Engineers, Hydrologic Engineering .

Commandre, B., En-Nejjary, D., Pibre, L., Chaumont, M., Delenne, C., Chahinian, N., 2017. Manhole cover localization in aerial images with a deep learning approach, in: ISPRS Hannover Workshop: HRIGI 17–CMRT 17–ISA 17–EuroCOW 17, pp. 333–338. doi:http://dx.doi.org/10.5194/isprs-archives-XLII-1-W1-333-2017.

Dasgupta, A., Grimaldi, S., Ramsankaran, R., Pauwels, V.R., Walker, J.P., 2022. A simple framework for calibrating hydraulic flood inundation models using crowd-sourced water levels. Journal of Hydrology 614, 128467. doi:10.1016/j.jhydrol.2022.128467.

DassFlow, 2019. Data Assimilation for Free Surface Flows. Technical Report. Mathematics Institute of Toulouse-INSA group-C&S corp.-CNES-CNRS. URL: http://www.math.univ-toulouse.fr/DassFlow.

Dellinger, G., Guiot, L., Pujol, L., Lawniczak, F., François, P., Finaud-Guyot, P., Vazquez, J., Garambois, P.A., in prep. Benchmark of hydrodynamic models for urban floods modeling in steady flow. .

Douvinet, J., Gisclard, B., Kouadio, J.S., Saint-Martin, C., Martin, G., 2017. Une place pour les technologies smartphones et les Réseaux Sociaux Numériques (RSN) dans les dispositifs institutionnels de l'alerte aux inondations en France? Cybergeo: European Journal of Geography doi:10.4000/cybergeo.27875.

Fabio, P., Aronica, G.T., Apel, H., 2010. Towards automatic calibration of 2-D flood propagation models. Hydrology and Earth System Sciences 14, 911–924. doi:10.5194/hess-14-911-2010.

Finaud-Guyot, P., Garambois, P.A., Araud, Q., Lawniczak, F., François, P., Vazquez, J., Mosé, R., 2018. Experimental insight for flood flow repartition in urban areas. Urban Water Journal 15, 242–250. doi:10.1080/1573062X.2018.1433861.

Finaud-Guyot, P., Garambois, P.A., Dellinger, G., Lawniczak, F., François, P., 2019. Experimental characterization of various scale hydraulic signatures in a flooded branched street network. Urban Water Journal 16, 609–624. doi:10.1080/1573062X.2020.1713173.

Galland, J.C., Goutal, N., Hervouet, J.M., 1991. TELEMAC: A new numerical model for solving shallow water equations. Advances in Water Resources 14, 138–148. doi:https://doi.org/10.1016/0309-1708(91)90006-A.

Garambois, P.A., Larnier, K., Monnier, J., Finaud-Guyot, P., Verley, J., Montazem, A.S., Calmant, S., 2020. Variational estimation of effective channel and ungauged anabranching river discharge from multi-satellite water heights of different spatial sparsity. Journal of Hydrology 581, 124409. doi:10.1016/j.jhydrol.2019.124409.

Garambois, P.A., Monnier, J., 2015. Inference of effective river properties from remotely sensed observations of water surface. Advances in Water Resources 79, 103–120. doi:10.1016/j.advwatres.2015.02.007.

Gochis, D., Barlage, M., Dugger, A., FitzGerald, K., Karsten, L., McAllister, M., McCreight, J., Mills, J., RafieeiNasab, A., Read, L., et al., 2018. The WRF-Hydro modeling system technical description. Version (5.1.1) URL: https://ral.ucar.edu/projects/wrf_hydro/documentation/wrf-hydro-v511-documentation.

Godunov, S., Bohachevsky, I., 1959. Finite difference method for numerical computation of discontinuous solutions of the equations of fluid dynamics. Matematičeskij sbornik 47, 271–306. URL: https://hal.archives-ouvertes.fr/hal-01620642.

Haile, A.T., Rientjes, T., 2005. Effects of LiDAR DEM resolution in flood modelling: A model sensitivity study for the city of Tegucigalpa, Honduras. Isprs wg iii/3, iii/4 3, 12–14. URL: https://www.isprs.org/proceedings/xxxvi/3-w19/papers/168.pdf.

Hascoet, L., Pascual, V., 2013. The Tapenade automatic differentiation tool: principles, model, and specification. ACM Transactions on Mathematical Software (TOMS) 39, 1–43. doi:10.1145/2450153.2450158.

Hocini, N., Payrastre, O., Bourgin, F., Gaume, E., Davy, P., Lague, D., Poinsignon, L., Pons, F., 2021. Performance of automated methods for flash flood inundation mapping: a comparison of a digital terrain model (DTM) filling and two hydrodynamic methods. Hydrology and Earth System Sciences 25, 2979 – 2995. doi:10.5194/hess-25-2979-2021.

Hostache, R., Lai, X., Monnier, J., Puech, C., 2010. Assimilation of spatially distributed water levels into a shallow-water flood model. Part II: Use of a remote sensing image of Mosel River. Journal of Hydrology 390, 257–268. URL: https://hal.inrae.fr/hal-02596687v1.

Jodeau, M., Hauet, A., Le Coz, J., Bodart, G., 2019. Fudaa-LSPIV Version 1.7. 1 User Manual. Lyon: IRSTEA France URL: https://forge.irstea.fr/projects/fudaa-lspiv/files.

Lamboni, M., Iooss, B., Popelin, A.L., Gamboa, F., 2013. Derivative-based global sensitivity measures: General links with Sobol' indices and numerical tests. Mathematics and Computers in Simulation 87, 45–54. doi:10.1016/j.matcom.2013.02.002.

Larnier, K., Monnier, J., Garambois, P.A., Verley, J., 2021. River discharge and bathymetry estimation from SWOT altimetry measurements. Inverse Problems in Science and Engineering 29, 759–789. doi:10.1080/17415977.2020.1803858.

Li, W., Wang, D., Liu, S., Zhu, Y., 2019. Measuring urbanization-occupation and internal conversion of peri-urban cultivated land to determine changes in the peri-urban agriculture of the black soil region. Ecological Indicators 102, 328–337. doi:10.1016/j.ecolind.2019.02.055.

Masson-Delmotte, V., Zhai, P., Pörtner, H.O., Roberts, D., Skea, J., Shukla, P.R., et al., 2022. Global Warming of 1.5 C: IPCC special report on impacts of global warming of 1.5 C above pre-industrial levels in context of strengthening response to climate change, sustainable development, and efforts to eradicate poverty. Cambridge University Press. doi:10.1017/9781009157940.

Mattheuwsen, L., Vergauwen, M., 2020. Manhole cover detection on rasterized mobile mapping point cloud data using transfer learned fully convolutional neural networks. Remote Sensing 12, 3820. doi:10.3390/rs12223820.

Mignot, E., Dewals, B., 2022. Hydraulic modelling of inland urban flooding: recent advances. Journal of Hydrology , 127763doi:10.1016/j.jhydrol.2022.127763.

Monnier, J., Couderc, F., Dartus, D., Larnier, K., Madec, R., Vila, J.P., 2016. Inverse algorithms for 2D shallow water equations in presence of wet dry fronts: Application to flood plain dynamics. Advances in Water Resources 97, 11–24. doi:10.1016/j.advwatres.2016.07.005.

Morris, M.D., 1991. Factorial Sampling Plans for Preliminary Computational Experiments. Technometrics 33, 161–174. URL: http://www.jstor.org/stable/1269043.

Neal, J.C., Bates, P.D., Fewtrell, T.J., Hunter, N.M., Wilson, M.D., Horritt, M.S., 2009. Distributed whole city water level measurements from the Carlisle 2005 urban flood event and comparison with hydraulic model simulations. Journal of Hydrology 368, 42–55. doi:10.1016/j.jhydrol.2009.01.026.

Nguyen, T.H., Ricci, S., Piacentini, A., Fatras, C., Kettig, P., Blanchet, G., Peña Luque, S., Baillarin, S., 2022. Dual State-Parameter Assimilation of SAR-Derived Wet Surface Ratio for Improving Fluvial Flood Reanalysis. Water Resources Research 58, e2022WR033155. doi:10.1029/

2022WR033155.

Ogden, F., Lai, W., Steinke, R., 2015. ADHydro: Quasi-3D high performance hydrological model. Proc. SEDHYD , 19–23.

Ogden, F.L., Raj Pradhan, N., Downer, C.W., Zahner, J.A., 2011. Relative importance of impervious area, drainage density, width function, and subsurface storm drainage on flood runoff from an urbanized catchment. Water Resources Research 47. doi:10.1029/2011WR010550.

Pujol, L., Garambois, P.A., Finaud-Guyot, P., Monnier, J., Larnier, K., Mose, R., Biancamaria, S., Yesou, H., Moreira, D., Paris, A., et al., 2020. Estimation of multiple inflows and effective channel by assimilation of multi-satellite hydraulic signatures: The ungauged anabranching Negro River. Journal of Hydrology 591, 125331. doi:10.1016/j.jhydrol.2020.125331.

Pujol, L., Garambois, P.A., Monnier, J., 2022. Multi-dimensional hydrological-hydraulic model with variational data assimilation for river networks and floodplains. EGUsphere 2022, 1–44. doi:10.5194/egusphere-2022-10.

Saltelli, A., Ratto, M., Andres, T., Campolongo, F., Cariboni, J., Gatelli, D., Saisana, M., Tarantola, S., 2008. Global sensitivity analysis: the primer. John Wiley & Sons.

Salvati, L., Quatrini, V., Barbati, A., Tomao, A., Mavrakis, A., Serra, P., Sabbi, A., Merlini, P., Corona, P., 2016. Soil occupation efficiency and landscape conservation in four Mediterranean urban regions. Urban Forestry Urban Greening 20, 419–427. doi:10.1016/j.ufug.2016.10.006.

Smith, M., Patrick, N., Frazier, N., Kim, J., 2021. Validation of Urban Flood Inundation Models Applied Using Nationally Available Data Sets: Novel Analyses of Observed High Water Information. Journal of Hydrologic Engineering 26, 04021039. doi:10.1061/(ASCE)HE.1943-5584.0002129.

Sobol', I., 2001. Global sensitivity indices for nonlinear mathematical models and their monte carlo estimates. Mathematics and Computers in Simulation 55, 271–280. doi:10.1016/S0378-4754(00)00270-6. The Second IMACS Seminar on Monte Carlo Methods.

Sobol', I., Kucherenko, S., 2009. Derivative based global sensitivity measures and their link with global sensitivity indices. Mathematics and Computers in Simulation 79, 3009–3017. doi:10.1016/j.matcom.2009.01.023.

Toro, E.F., 2013. Riemann solvers and numerical methods for fluid dynamics: a practical introduction. Springer Science & Business Media.

Zhang, X., Chen, J., Tan, M., Sun, Y., 2007. Assessing the impact of urban sprawl on soil resources of Nanjing city using satellite images and digital soil databases. CATENA 69, 16–30. doi:10.1016/j.catena.2006.04.020.

Zhu, C., Byrd, R.H., Lu, P., Nocedal, J., 1997. Algorithm 778: L-BFGS-B: Fortran subroutines for large-scale bound-constrained optimization. ACM Transactions on Mathematical Software (TOMS) 23, 550–560. doi:10.1145/279232.279236.